

**AFRL-AFOSR-UK-TR-2012-0004**



## **Attenuation of Vane-Rotor Shock Interactions with Pulsating Coolant Flows**

**Guillermo Paniagua**

**Institut von Karman de Dynamique des Fluides  
Waterloosesteenweg 72  
Rhode-St-Genese  
Sint Genesius Rode, Belgium B-1640**

EOARD GRANT 08-3033

Report Date: March 2012

Final Report for 01 August 2008 to 01 August 2011

**Distribution Statement A: Approved for public release distribution is unlimited.**

**Air Force Research Laboratory  
Air Force Office of Scientific Research  
European Office of Aerospace Research and Development  
Unit 4515 Box 14, APO AE 09421**

**REPORT DOCUMENTATION PAGE**

Form Approved OMB No. 0704-0188

Public reporting burden for this collection of information is estimated to average 1 hour per response, including the time for reviewing instructions, searching existing data sources, gathering and maintaining the data needed, and completing and reviewing the collection of information. Send comments regarding this burden estimate or any other aspect of this collection of information, including suggestions for reducing the burden, to Department of Defense, Washington Headquarters Services, Directorate for Information Operations and Reports (0704-0188), 1215 Jefferson Davis Highway, Suite 1204, Arlington, VA 22202-4302. Respondents should be aware that notwithstanding any other provision of law, no person shall be subject to any penalty for failing to comply with a collection of information if it does not display a currently valid OMB control number.

**PLEASE DO NOT RETURN YOUR FORM TO THE ABOVE ADDRESS.**

<b>1. REPORT DATE (DD-MM-YYYY)</b> 23-03-2012	<b>2. REPORT TYPE</b> Final Report	<b>3. DATES COVERED (From - To)</b> 1 August 2008 - 01 August 2011
--	---------------------------------------	---

<b>4. TITLE AND SUBTITLE</b>  <b>Attenuation of Vane-Rotor Shock Interactions with Pulsating Coolant Flows</b>	<b>5a. CONTRACT NUMBER</b> FA8655-08-1-3033
	<b>5b. GRANT NUMBER</b> <b>Grant 08-3033</b>
	<b>5c. PROGRAM ELEMENT NUMBER</b> 61102F

<b>6. AUTHOR(S)</b>  Professor Guillermo Paniagua	<b>5d. PROJECT NUMBER</b>
	<b>5d. TASK NUMBER</b>
	<b>5e. WORK UNIT NUMBER</b>

<b>7. PERFORMING ORGANIZATION NAME(S) AND ADDRESS(ES)</b> Institut von Karman de Dynamique des Fluides Waterloosesteenweg 72 Rhode-St-Genese Sint Genesius Rode, Belgium B-1640	<b>8. PERFORMING ORGANIZATION REPORT NUMBER</b>  N/A
---	--

<b>9. SPONSORING/MONITORING AGENCY NAME(S) AND ADDRESS(ES)</b>  EOARD Unit 4515 BOX 14 APO AE 09421	<b>10. SPONSOR/MONITOR'S ACRONYM(S)</b> AFRL/AFOSR/RSW (EOARD)
	<b>11. SPONSOR/MONITOR'S REPORT NUMBER(S)</b> <b>AFRL-AFOSR-UK-TR-2012-0004</b>

**12. DISTRIBUTION/AVAILABILITY STATEMENT**  
Approved for public release; distribution is unlimited.

**13. SUPPLEMENTARY NOTES**

**14. ABSTRACT**  
A transonic turbine airfoil was experimentally and numerically tested to resolve the effects of pulsating cooling. The model was tested at four Mach numbers (0.8, 0.95, 1.1, and 1.2), and two engine representative Reynolds numbers ( $4 \times 10^6$  and  $6 \times 10^6$ ). The detrimental effects of the trailing edge shock waves on the neighboring airfoil and downstream plane are reduced with coolant ejection. The highest reduction is achieved with pulsating cooling. The Reynolds number stabilized the shock angle, minimized the RMS. Pulsating cooling ejection results in shock waves less oblique with significantly lower RMS values. A detailed investigation of the flow topology at the base region shows the modes of vortex shedding for different main flow and cooling conditions. The frequency of the vortex shedding is increased by introducing coolant which first pushes the vortex formation location downstream and at high ejection rates divides the base region into two. Surface temperatures were extracted on the suction side by using fast response thin film gauges. Nusselt number distributions were extracted to designate the location of boundary layer transition. Unsteadiness associated with blade temperature were reported in terms of signal RMS. The result of the analyses shows significant agreement and complements each other in determination of the inclination and the intensity of the shock waves changing with cooling condition. It has been observed that the shock angle is increased and intensity is decreased by increasing coolant ejection pressure within the range of interest. The highest improvement in terms of the impact on the neighboring airfoil is attained with pulsating cooling. In addition, the stabilizing effect of pulsating coolant ejection is observed on boundary layer unsteadiness. Base pressure is observed to be highly affected by the base bleed. The value is increased the most by a low coolant ejection rate. Pulsating cooling maintains the base pressure at the same level of the continuous cooling with the same average ejection pressure. The impact of cooling on wake unsteadiness for various Mach and Reynolds numbers are quantified in terms of the Strouhal number. The present novel research on control of the shock waves presents the influence of unsteady trailing edge coolant ejection on the modulation of shock waves. The potential implementation of the proposed cooling scheme in turbine applications might lead to turbine efficiency and life-span increase. Furthermore, the present results should provide aerodynamic designers new tools to harness shock interactions.

**15. SUBJECT TERMS**  
EOARD, Aerodynamics, Turbomachinery

<b>16. SECURITY CLASSIFICATION OF:</b>			<b>17. LIMITATION OF ABSTRACT</b>  SAR	<b>18. NUMBER OF PAGES</b>  23	<b>19a. NAME OF RESPONSIBLE PERSON</b> Gregg Abate
<b>a. REPORT</b> UNCLAS	<b>b. ABSTRACT</b> UNCLAS	<b>c. THIS PAGE</b> UNCLAS			<b>19b. TELEPHONE NUMBER (Include area code)</b> +44 (0)1895 616021

Contract FA8655-08-1-3033

PROJECT TITLE:  
Attenuation of Vane-Rotor Shock Interactions  
With Pulsating Coolant Flows

B.H. Saracoglu, Dr. G. Paniagua  
von Karman Institute for Fluid Dynamics

**Distribution A: Approved for public release; distribution is unlimited.**

## SUMMARY

In transonic and supersonic turbomachinery, shock waves appear at the trailing edge, generating substantial losses due to the interaction with the boundary layer. A novel proposal to control the resulting fish tail shock waves consists on, pulsating coolant blowing through the trailing edge of the airfoils. This paper presents an unprecedented experimental and numerical research. A linear cascade representative of modern turbine bladings was specifically designed and constructed. The test matrix comprised four Mach numbers, from subsonic to supersonic regimes (0.8, 0.95, 1.1 and 1.2) together with two engine representative Reynolds numbers ( $4$  and  $6 \times 10^6$ ) at various blowing rates. The blade loading and the downstream pressure distributions allowed understanding the effects on each leg of the shock structure. Heat transfer measurements were performed to quantify the consequences of different coolant blowing schemes. Shock angle variation and intensity reduction has been quantified at different cooling rates. Shock induced boundary layer transition has been identified with both continuous and pulsating coolant ejection. Minimum shock intensities were achieved using pulsating cooling. A substantial increase in base pressure was observed for low coolant blowing rate. Analysis of the high frequency Schlieren pictures revealed the modulation of the shock waves with the coolant pulsation. The Strouhal number of the vortex shedding was analyzed for all of the conditions.

SUMMARY .....	2
1. Introduction.....	4
2. Experimental apparatus.....	5
2.1. Airfoil model.....	5
2.2. Wind tunnel.....	5
2.3. Rotating valve .....	6
2.4. Measurement techniques.....	7
3. Numerical tool .....	9
3.1. Description of the solver .....	9
3.2. Computational domain and parameters of the analysis .....	9
4. Shock modulation .....	10
4.1. Operating conditions .....	10
4.2. Airfoil loading.....	10
4.3. Downstream static pressure .....	12
4.4. Shock angle fluctuations .....	12
4.5. Steady wall temperature.....	13
4.6. Unsteady wall temperature.....	14
5. Base pressure .....	15
5.1. Base region flow topology and vortex shedding.....	15
5.2. Base pressure correlation .....	18
6. Conclusions.....	19
References.....	19

## 1. Introduction

Trailing edge shock interactions are one of the major sources of losses in supersonic airfoils. Additionally, vane shocks cause large pressure fluctuations that may result in low and high cycle fatigue problems. Previous research related to the present investigation may be classified in four topics: trailing edge shock wave interactions, base pressure losses, trailing edge vortex shedding, and effects of the coolant ejection.

The downstream flow field of nozzle guide vanes in modern high pressure turbines suffers fish tail shock structures [1]. The trailing edge shock pattern has been well documented in the literature. Denton and Xu [2, 3] quoted that the trailing edge losses contribute typically to a third of the total losses in transonic turbines. The impingement of those compression waves on the downstream rotor row and rear suction side of the adjacent vane results in unsteady entropy generation. Quantification of unsteady loss and pressure variation in a transonic turbine was studied numerically and experimentally in the literature [4].

Regarding the base pressure losses Gostelow et al. [5] analyzed computationally and experimentally the trailing edge structure and the related losses. Uzol et al. [6, 7] documented the performance of different trailing edge geometries. Schobeiri and Pappu [8] found an optimal geometry and blowing ratio that minimize the mixing losses of a cooled gas turbine blade. Sieverding et al. [9] determined an experimental correlation of the base pressure in function of the downstream static pressure, that allows accurate predictions of base pressure losses.

Concerning the vortex shedding, Rowe et al. [10] observed that a thick boundary layer upstream of the trailing edge reduced the shedding frequency, resulting in decreased base pressure losses. Sieverding and Heinemann [11] demonstrated the influence on the vortex shedding of the boundary layer state on both pressure and suction sides. Furthermore, the vortex street exhibits a 2D structure only in the midspan region [12]. Cicitelli and Sieverding [13] characterized experimentally the time averaged and unsteady pressure field in the base region.

Studies on the effect of coolant ejection on the vortex shedding were presented by Motallebi and Norbury [14] based on Schlieren images of the vortices shed from a blunt trailing edge at subsonic and supersonic conditions. A certain rise in the base pressure was noticed corresponding to a moderate coolant flow rate. The disappearance of the trailing edge vortex motion was observed over a range of bleed air mass flows near to the value producing a maximum level of base pressure. Sieverding [15] showed that a higher base pressure and a consequent reduction of the trailing edge shock intensity corresponded to a moderate coolant flow rate. Raffel and Kost [16] gathered similar results at supersonic conditions using PIV data. Saracoglu et al. [17] obtained analogous conclusions using numerical simulations on a blunt trailing edge at an outlet Mach equal to 1.5, the shock strength was mitigated 70% at moderate trailing edge cooling compared to the no blowing case.

In conjunction with Paniagua et al. [4], de la Loma et al. performed numerical and experimental heat transfer measurements on a transonic turbine stage to show the loss and unsteady forcing mechanism due to vane trailing edge shocks [18]. Further heat transfer measurements were performed by Solano et al. in a radial transonic turbine rig to predict the flow structures from blade Nusselt number distributions [19].

The research has demonstrated that cooling ejection has significant effects on the base region and trailing edge shock patterns. The originality of this work lies in the use of pulsating coolant to control shocks for the first time in the literature. Experimental and numerical research have been performed to understand the base region flow topology depending on cooling ejection rates. Several correlations for the base pressure, shock angle and vortex shedding are presented. The current study demonstrates that cooling ejection has significant effects on trailing edge shock patterns and consequently their effects on the adjacent blade's boundary layer properties by using pressure and heat transfer measurements in coordination. The final goal of the research is to improve turbine durability and efficiency in compact supersonic turbomachinery. This paper may guide aerodynamic designers to novel concepts to modulate shock waves.

## 2. Experimental apparatus

### 2.1. Airfoil model

The airfoil model reproduces the velocity distribution encountered in a modern cooled turbine airfoil. The trailing edge diameter was maximized to increase the spatial and temporal resolution of the vortex shedding phenomena in the Schlieren flow visualizations. The rear part of the suction side was identical to the airfoil documented by Sieverding et al. [20], as shown in Fig. 1. The rest of the profile was fitted by high-order Bézier curves to ensure the continuity of the curvature and passage width, resulting in a smooth velocity evolution.

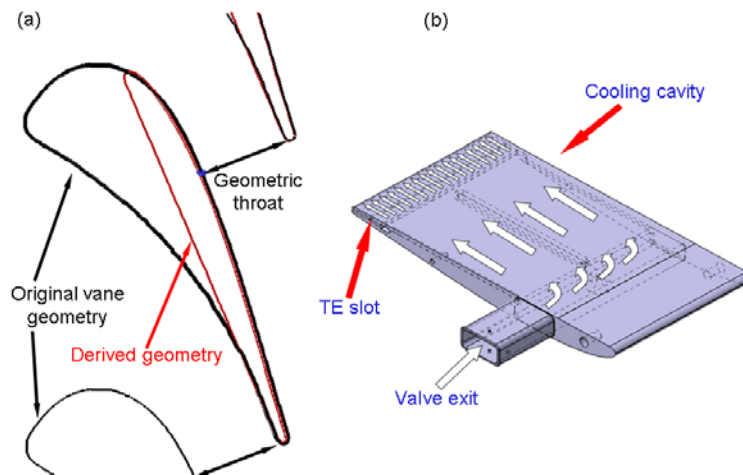


**Fig. 1.** a) The construction of the airfoil geometry b) Internally cooled airfoil

The aerodynamic performance of the cascade passage was tested for various downstream isentropic Mach numbers, ranging from 0.8 to 1.2. The flow field around the airfoil leading edge was investigated in detail to analyze incidence effects. No sign of separation was observed for the incidence angles of  $\pm 2$  degrees.

### 2.2. Wind tunnel

An isentropic compression tube facility at the von Karman Institute has been used to perform all experiments in this work (Fig. 2). Optical access detailed in Fig. 5

permitted Schlieren and oil flow visualizations. The facility provides 100 to 800 ms of testing time [b19, b20]. The test duration varies exponentially with the test Reynolds number (Fig. 3).

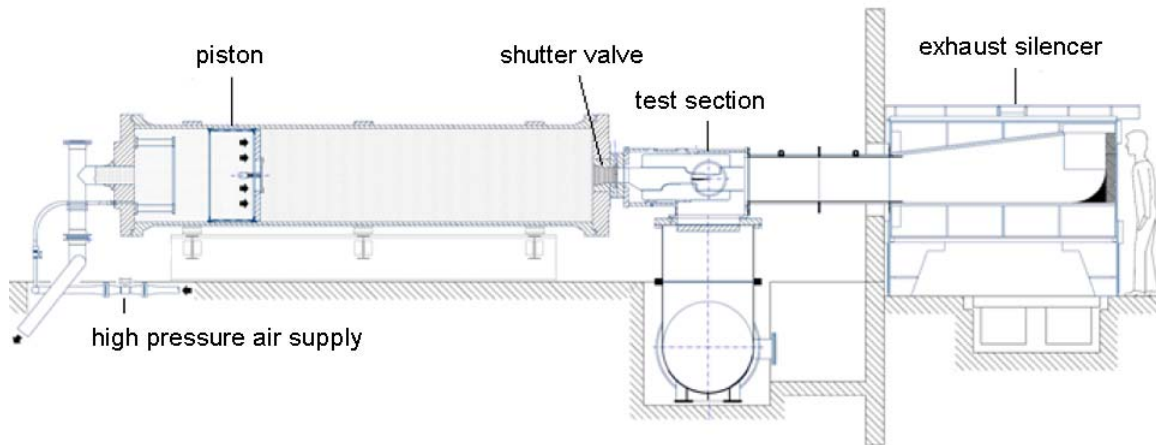


**Fig. 2.** The schematic of the experimental facility

The air inside the cylindrical vessel is compressed by a free piston driven by high pressure dry air (300 bars) until the desired upstream conditions are attained. Subsequently, a shutter valve releases the air into the test section. The flow is vented axially to the atmosphere.

The test section accommodates two flow passages separated by an airfoil. The model and two contoured end wall sections are staggered at 66 degrees. Transonic flow adaptation is achieved by a sudden expansion downstream of the trailing edge.

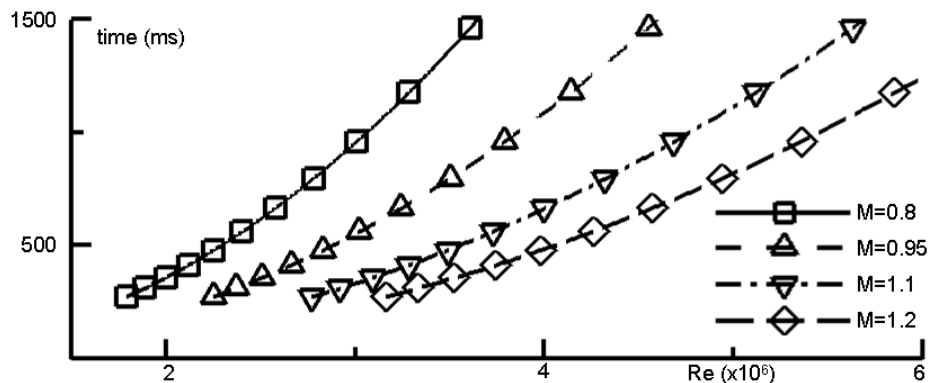


**Fig. 3.** Testing time changing for different test conditions (Reynolds and Mach number)

### 2.3. Rotating valve

Pulsation in the coolant stream was provided by a perforated rotating disc. When the holes on the disc are facing the inlet and outlet ducts a flow pulse is generated. Detailed characterization of the rotating valve cooling system was performed upstream and downstream of the airfoil [23]. The mean mass flow rate in function of upstream total pressure is displayed in Fig. 4 – left at various frequencies. Fig. 4 – right depicts the temporal evolution of the mass flow, for a given coolant pressure of 1.9 bars at 200 Hz.

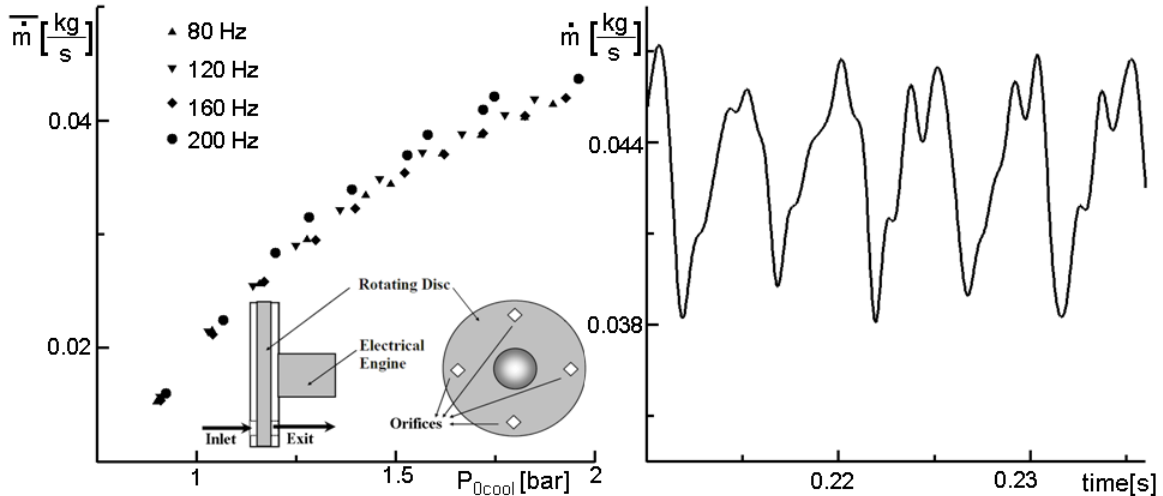


**Fig. 4.** Mean coolant mass flow rate with respect to coolant total pressure at various frequencies (left), mass flow fluctuations with pulsating cooling (right)

#### 2.4. Measurement techniques

Measurements were performed at several locations along the test section. The inlet total pressure and temperature were measured with a Pitot probe and K-type micro thermocouple (25  $\mu$ m) located one chord upstream of the airfoil leading edge. The probe head was at 30% of the inlet channel height.

The model and the adjacent suction and pressure sides are equipped with pneumatic lines at mid-span. The first passage (in Fig. 5-b) contains 13 taps on the lower wall (pressure side) as well as 13 taps on the model suction side. Similarly, the second passage has 6 taps on the airfoil (pressure side) and 14 taps on the upper wall (suction side). Additionally, 5 piezoresistive sensors are installed on the model. The trailing edge was instrumented with two piezoresistive sensors and two pneumatic lines located at each side of the cooling slot.

The outlet pitch-wise pressure distribution was monitored by a row of pneumatic taps located at 25% of the chord downstream of the trailing edge plane, consisting of 12 taps over 80% of the pitch. All pneumatic lines were sampled with 1.1 bar ScaniValve sensors at a sampling rate of 300 Hz, whereas the piezoresistive sensors were recorded at 500 kHz. The measurements were averaged for a constant time interval when the stable operating conditions were achieved to attain the time-averaged quantities. Fig. 5-a displays the Mach number evolution in a typical experiment.

High speed Schlieren flow visualizations were performed with the Z-type Schlieren setup [24]. The 800x600 pixel resolution pictures were acquired at a rate of 3200 Hz by a Phantom V9 high-speed camera. A digital image processing algorithm was developed in Matlab<sup>®</sup> to analyze the images. Each single image was automatically rotated and cropped around the area of interest. A local background was created and subtracted from the image to compensate for illumination variations. The algorithm converted this image portion into a binary image, i.e. a logical array, and tagged its connected components providing a label matrix, where each object was identified with a positive integer number. The geometrical properties of the detected objects were obtained by measuring the characteristics of each labeled component in the label matrix. Eccentricity was used as criterion to select the one that corresponds to the compression wave among

the detected items. The center and the orientation of the wave were then stored for further investigation. Spectral analysis of the Schlieren images allowed identifying the shock displacement frequency and angle variation amplitude. The impingement location of the shock wave on the adjacent suction surface was also extracted as complementary information for the blade loading measurements.

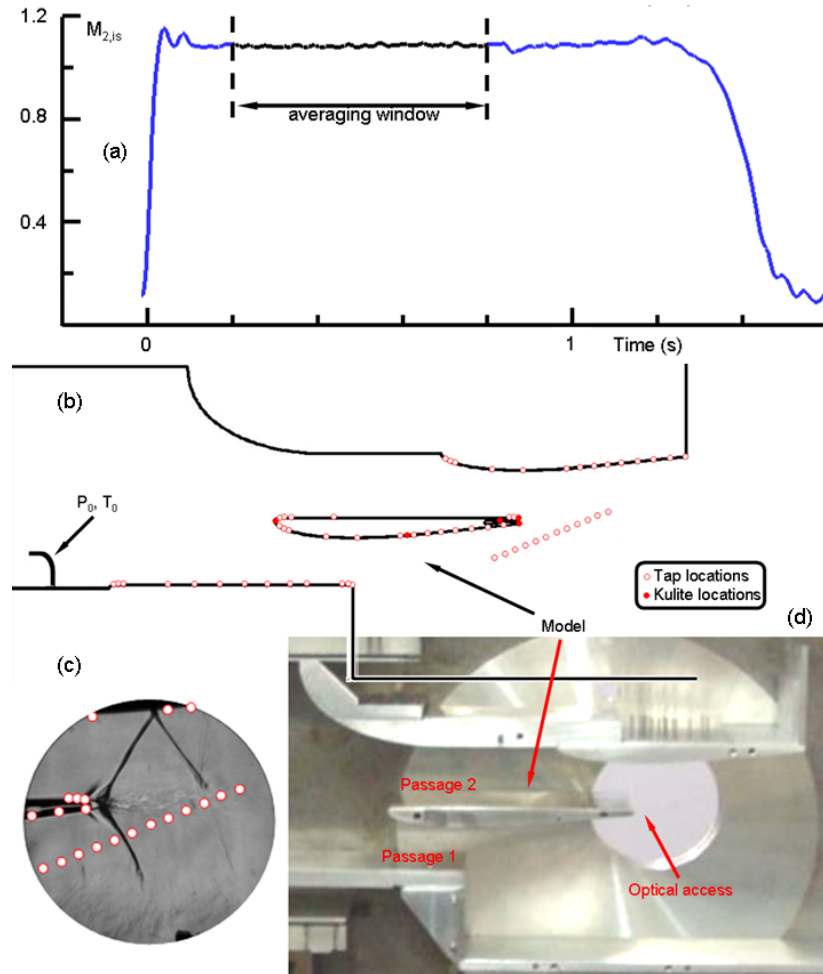


**Fig. 5.** a) Variation of downstream isentropic Mach number during a test; b) Schematic view of the test section with pressure measurement locations; c) Schlieren picture together with pressure sensor taps; d) Manufactured test set-up

Steady and unsteady surface temperature measurements were performed on the suction side contoured top wall of the test section to assess the disturbances on the boundary layer by using 11 nickel based thin film sensors fabricated by Tao Systems (Fig. 6). The entire unsteady data acquisition was done at sampling frequency of 1 MHz. The part of the sampled data which falls into the constant main flow condition time interval was used for processing. The wall temperature signals acquired by thin film sensors were decomposed into mean and fluctuating components. The mean value was used to calculate the heat flux by solving 1D heat conduction equation while substrate of the sensors considered as semi-infinite medium. Following this procedure, the heat transfer coefficient  $h$  was calculated by using the wall and the gas temperatures. Finally,

Nusselt numbers for each sensor were calculated. The root mean square (RMS) of the temperature was extracted from the fluctuating component of signal to measure the level of unsteadiness in wall temperature on each gauge locations.

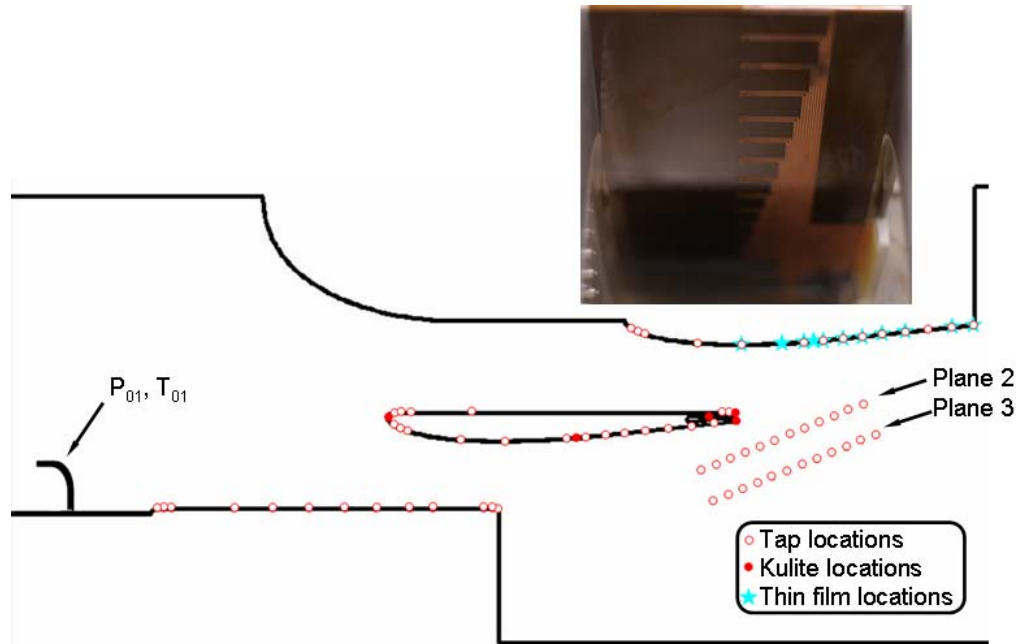


**Fig. 6.** Pressure and temperature measurement locations

### 3. Numerical tool

#### 3.1. Description of the solver

The commercial solver ANSYS FLUENT was used for all the simulations. The 2D version solved the governing equations using a co-located grid, i.e. all the flow parameters were stored in the cell-centers. Regarding the spatial discretization, a second order upwind scheme was selected for the present numerical campaign. A second order temporal discretization was used to obtain the time-accurate unsteady solutions. Gradients were reconstructed using a second order accurate method based on cell volumes. Turbulence was modeled using the two-equation SST model by Menter [25]. Calculations were performed using a parallelized approach on multiple computer nodes.

#### 3.2. Computational domain and parameters of the analysis

The numerical domain reproduced a single vane passage, as displayed in Fig. 7, considering periodic boundary conditions on the upper and lower ends of the domain. The inlet and outlet sections which were inclined according to the stagger angle of the linear cascade were located 0.5 and 0.75 chords away from the profile leading and trailing edges respectively. The computational mesh was prepared using the commercial tool Centaur. Special attention was paid to the resolution on the wall, the base and the wake regions. An O grid of 20 prismatic layers was realized around the blade. The resulting  $y^+$  value was maintained below 1 around the airfoil profile. The final mesh consisted of around 30,000 prismatic and 535,000 triangular elements. The imposed inlet total pressures, total temperatures, and flow angles corresponded to the experimental

values. At the outlet, the measured average static pressure  $P_{s2}$  was imposed. All the walls were assumed to be isothermal at ambient temperature with no-slip boundary condition. To model the pulsating coolant, a user-defined function was implemented with a pressure shape, similar to the experimental conditions documented by Gonzalez et al. [23], as depicted in Fig. 4-right.

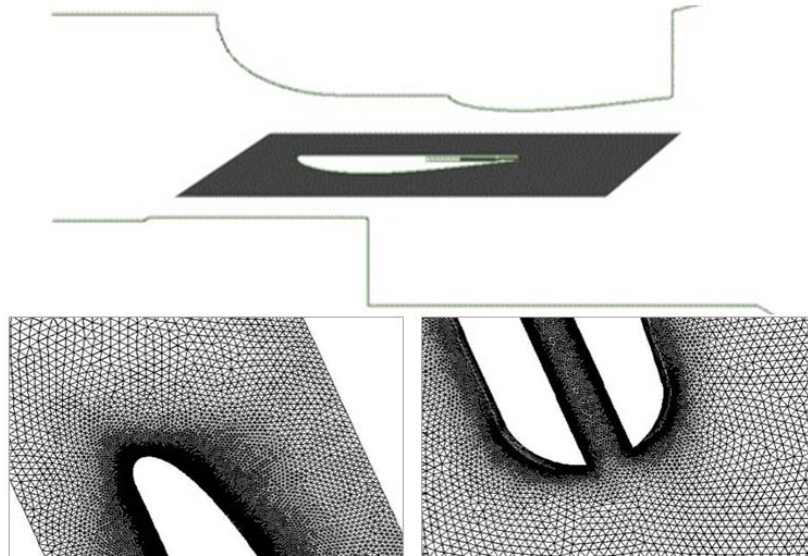


**Fig. 7.** Computational domain: as cropped from the test section (top) along with magnified views of the leading edge (bottom left) and trailing edge (bottom right)

In order to ensure a frequency resolution of 500 kHz, a time step of  $1 \mu\text{s}$  was used. Time averaged data was obtained by calculating the mean of 4 consecutive periods, after verifying that the level of dispersion was below a threshold. The analysis of the data with pulsating frequency (200 Hz) was accomplished using a time step ten times larger ( $10 \mu\text{s}$ ), because the typical period to resolve is 100 times greater. The computational time required to achieve full convergence was 1344 CPU hours in two processors, dual core AMD Opteron with 4GB RAM.

## 4. Shock modulation

### 4.1. Operating conditions

The tests were made for a range of high subsonic to low supersonic Mach numbers ( $M_{2,is}=0.8-1.2$ ), while 2 Reynolds numbers have been selected ( $Re=4 \times 10^6$  &  $6 \times 10^6$ ). All conditions were tested for no blowing and continuous blowing at 1.1, 1.5 and 1.9 bars of coolant total pressures ( $P_{0,cool}$ ). A pulsating coolant stream was introduced for transonic and supersonic test cases at an average coolant total pressure of 1.9 bars with a frequency of 200 Hz resulting in a 12% fluctuation of the mean coolant mass flow.

### 4.2. Airfoil loading

The analysis of the time-averaged pressure is performed to characterize the flow field aerodynamics in the cascade passage and the downstream planes. The pressure

values are represented in terms of isentropic Mach numbers ( $M_{is} = \sqrt{2/(\gamma - 1) \left( (P_{01}/P_s)^{(\gamma-1)/\gamma} - 1 \right)}$ ). Fig. 8 depicts the distributions with respect to normalized surface coordinate ( $S/S_{max}$  equals 0 at the leading edge and one at the trailing edge) on the upper flow passage for each test condition and for each coolant blowing pressure.

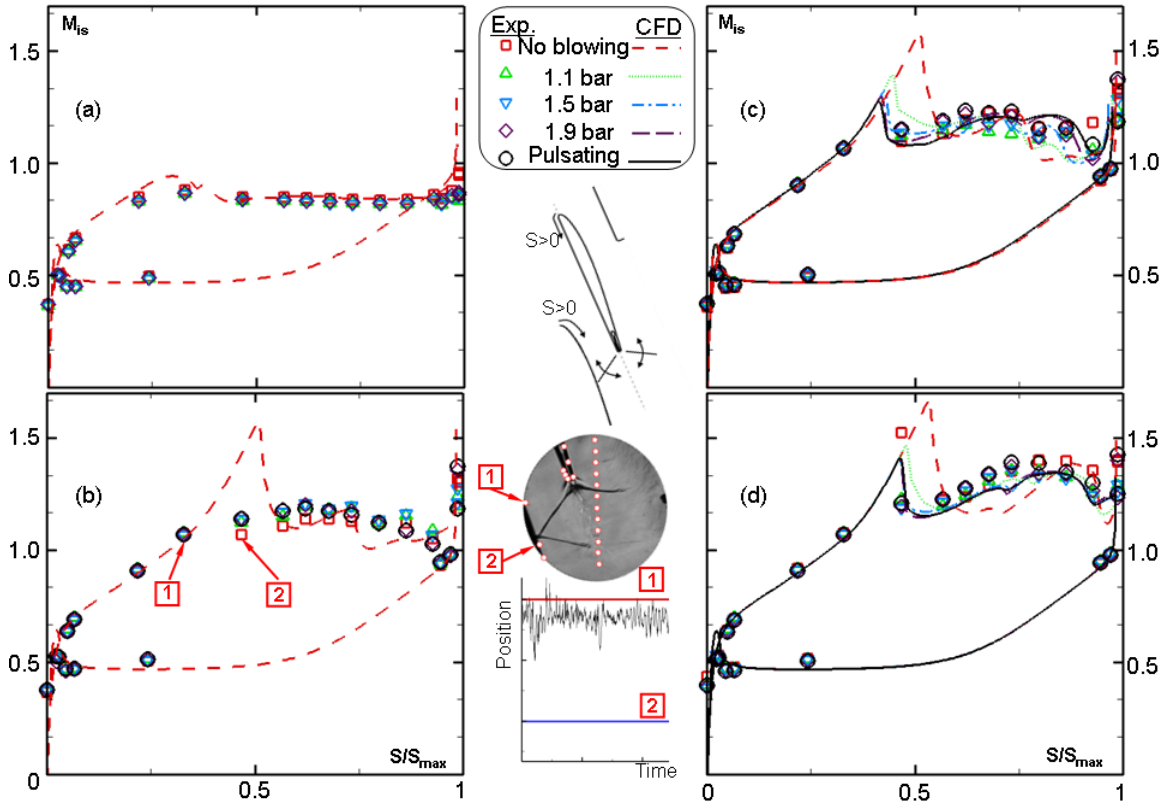


**Fig. 8.** The variation of velocity distribution of upper channel a)  $M_{2,is}=0.8$ ,  $Re=4 \times 10^6$ ; b)  $M_{2,is}=1.1$ ,  $Re=4 \times 10^6$ ; c)  $M_{2,is}=1.1$ ,  $Re=6 \times 10^6$ ; d)  $M_{2,is}=1.2$ ,  $Re=6 \times 10^6$

In Fig. 8-c we observe a large acceleration along the suction side in the leading edge region. From  $S/S_{max}$  0.05 to 0.3 (throat) there is a constant acceleration. Downstream of the throat the flow overaccelerates due to the expansion fan until the impact of the right running shock. After the deceleration caused by the shock wave, the flow keeps on accelerating downstream. The cooling scheme does not alter the pressure distribution around the profile for the cases below sonic speed. For supersonic outlet conditions, the coolant affects only the region downstream of the shock impingement. The behavior is not visible in the experimental results due to the fact that the impingement location of the shock wave statistically lies between two measurement locations denoted as 1 and 2 in Fig. 8 as revealed from the processing of Schlieren pictures. The CFD reveals an upstream displacement of the shock impact with the coolant mass flow. The increase of Mach number to 1.2 results in a substantial increase in the passage loading. One can also observe that the pulsating cooling results in lower loading than the continuous blowing.

### 4.3. Downstream static pressure

The pressure distributions on plane 2 provided an exact location of the left-running shock. Fig. 9 represents the downstream isentropic Mach numbers for supersonic conditions together with corresponding Schlieren images to illustrate the orientation of the left-running shock wave with respect to the measurement locations. The right running shock reflection effect can be seen at pitch-wise locations between  $g/g^*=1.35$  and  $g/g^*=1.5$ . For  $M_{2, is}=1.1$  and  $Re=4 \times 10^6$ , the pressure increase downstream of the right running shock reflection is reduced when the coolant is introduced. A similar effect is observed for the other cases as well. One can also notice that the shock wave is less oblique for  $M_{2, is}=1.2$  and  $Re=6 \times 10^6$  when the coolant is introduced.

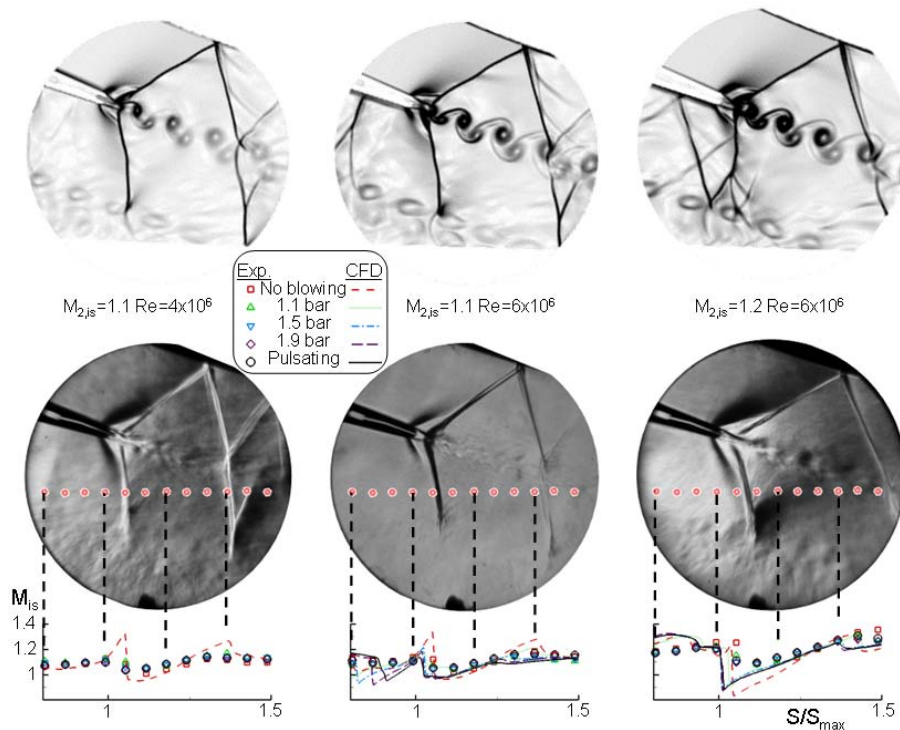


**Fig. 9.** Pitch-wise pressure distribution downstream of the cascade for all test conditions

### 4.4. Shock angle fluctuations

The analysis of the shock angle movement is based on the numerical and experimental Schlieren. Regarding the uncooled case, the shock angle varies between 55 to 60.5 deg. at the vortex shedding frequency (about 20 kHz). The use of pulsating cooling implies variations of about 5 degrees at the pulsating coolant frequency (about 200 Hz). Fig. 10 compares the power spectrum of the unsteady shock wave angle ( $\alpha$ ) with the valve encoder and the pressure sensor in the cooling slot ( $P_{cool}$ ). It is clear in both figures that the pulsating cooling at 208 Hz is altering the shock angle at exactly the same frequency.

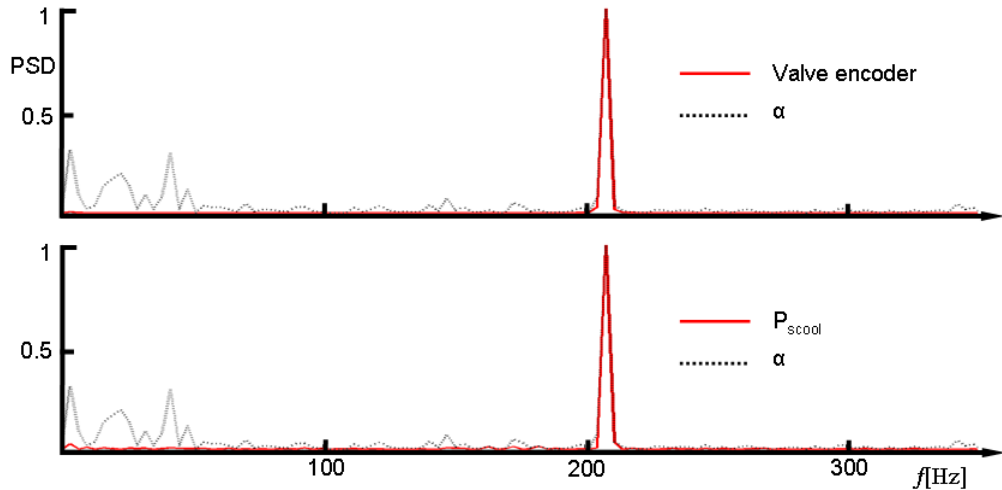


**Fig. 10.** Comparison of the experimental power spectrum of the shock wave angle variation with: Encoder delivering one pulse per revolution (top); high-frequency pressure sensor in the cooling slot (bottom)

In Fig. 11, the average angle variation obtained by the Schlieren images analysis is presented together with the corresponding RMS value. The mean angle and the variability of the shock waves are reduced by increasing the Mach number. Furthermore, increasing Reynolds number provide a stabilizing effect, or reduction of RMS, on the shock angle. The average shock angle and the RMS are observed to be decreased by the pulsating cooling.

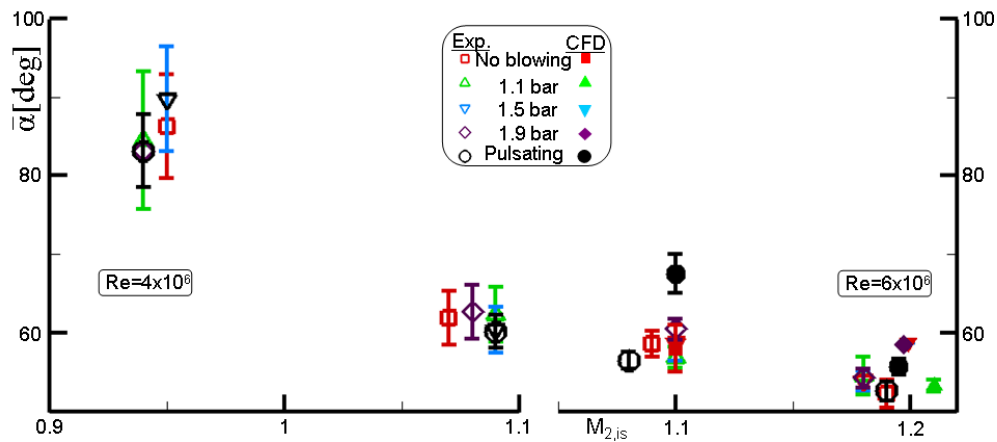


**Fig. 11.** Schlieren results: average angles with error bar (RMS) for all conditions

#### 4.5. Steady wall temperature

The Nusselt number distributions on the suction surface of the upper flow passage for various test conditions were calculated by using the time-averaged  $T_w$ ,  $T_{01}$ , wall heat flux and calculated main stream heat conduction coefficient and illustrated by the middle plot sequence in Fig. 12. A reduction in Nu is observed towards the downstream location of geometrical throat regardless of test condition. While laminar boundary layer thickens, it isolates the surface from heat penetration thus Nu decreases. Further downstream, an

increase in  $Nu$  is noticed as an indication of initiation of boundary layer transition. Following a finite length of  $Nu$  gradient, relatively constant region of  $Nu$  is observed on the rear suction side where the turbulent boundary layer establishes. For low  $M$  and  $Re$  case, the location of transition is detected on half way of the surface which is far downstream of the shock wave impingement point. This informs possible natural transition of the blade surface. Moreover, the transition is delayed 5%  $S_{max}$  when the coolant is blown pulsating. When freestream Mach number is increased, transition is moved 5%  $S_{max}$  upstream coinciding with the shock impingement location for a longer length. On the other hand, the increase in  $Re$  results in delay in transition to a location between 46% and 67%  $S_{max}$  for low coolant mass flows. Finally, boundary layer of highest Mach number case gets transitional for all cooling cases between 46% and 51%  $S_{max}$  where the shock wave impinges for all cooling schemes and gets turbulent between 67%  $S_{max}$ .

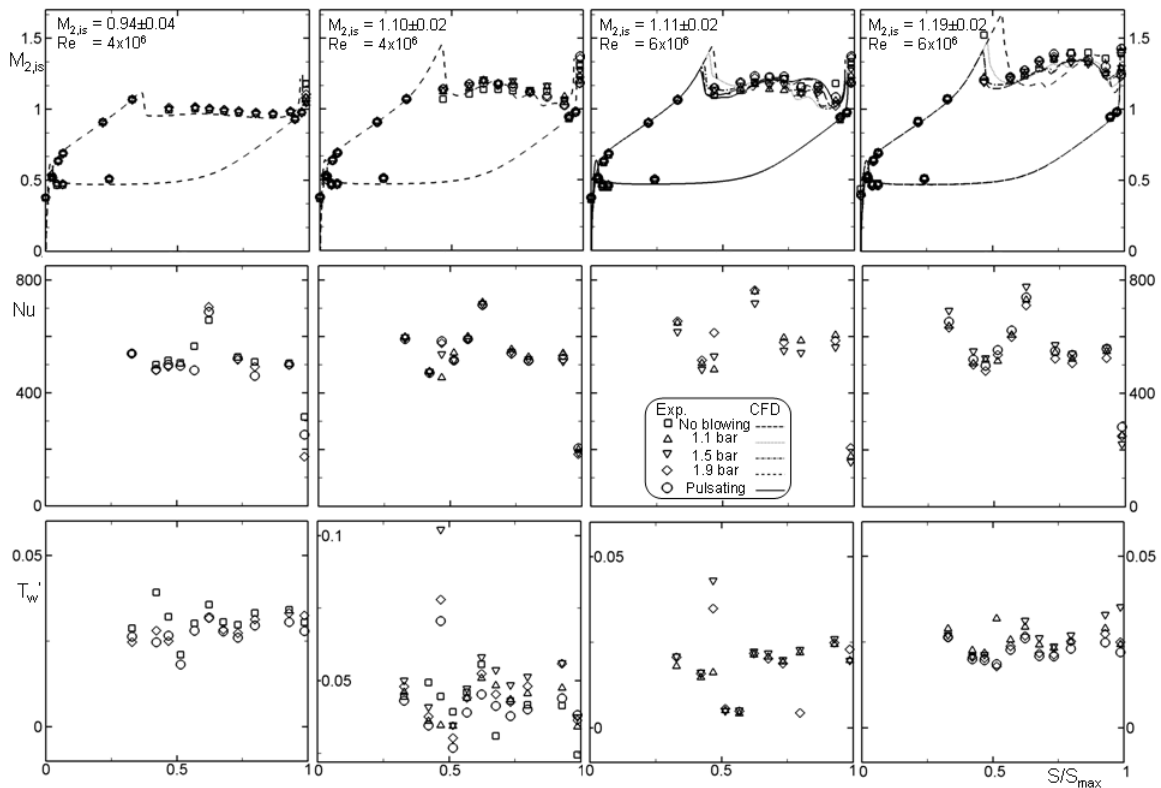


**Fig. 12.** Blade loading (top) together with suction side Nusselt number (middle) and RMS of wall temperature (bottom) distributions on the upper flow passage

#### 4.6. Unsteady wall temperature

The wall temperature signal can be split into a mean value and random fluctuations. The random component can be represented by the root mean square (RMS) of it throughout the time span. Consequently, the root mean squared value of the temperature represents the level of unsteadiness for each signal. Thus, the procedure was applied and resulted RMS distributions are represented in Fig. 12 bottom. A sudden increase in wall temperature unsteadiness was encountered at same location of the

beginning of transition depicted on Nu distribution and shock impingement point on blade loading for both free stream Reynolds numbers due to the relative increase in unsteadiness by transition from laminar to turbulent boundary layer. This behavior not only confirm the consistency of the results inferred from different measurements but also indicates lowest RMS values for unsteady cooling cases which might be an indication of stabilizing effect of pulsating coolant blowing by reducing shock intensity.

The frequency spectrum of the wall temperature signal has also been analyzed in order to characterize unsteady phenomenon occurring in the boundary layer for different test conditions. An example of the low frequency content of the wall temperature signal is given in Fig. 13 (left). A distinct peak at around 500 Hz with a dispersion of 50 Hz has consistently been observed for all of the gauges. The designated low frequency fluctuation might be a signature of the unsteadiness caused by large recirculation bubbles downstream of the end walls of the test section which has numerically diagnosed [26]. Similar frequencies were also captured by cooling channel pressure sensor in the absence of trailing edge blowing (Fig. 13. right).

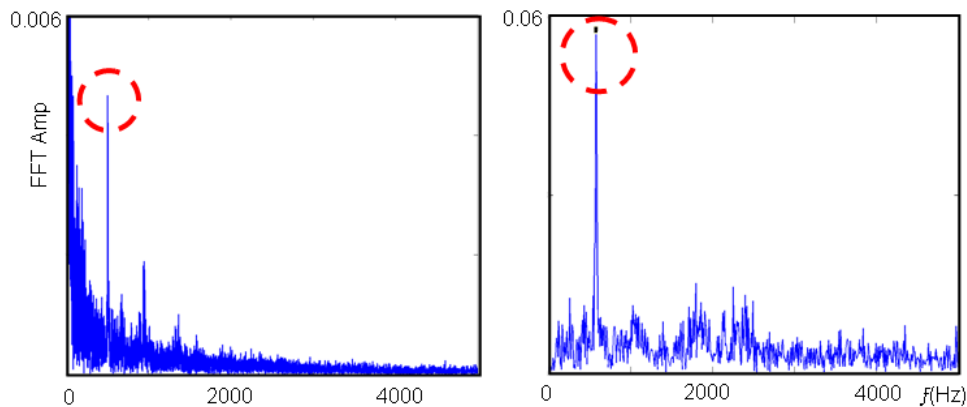


**Fig. 13.** FFT of wall temperature signal (left) edge and cooling channel pressure for no blowing case (right)

## 5. Base pressure

### 5.1. Base region flow topology and vortex shedding

Trailing edge cooling alters significantly the behavior of the vortex shedding. In the uncooled case, the coherent structures of the von Karman vortex street are clearly visible for both investigated Reynolds numbers (Fig. 14). Gostelow [27] stated that for transonic flows the von Karman vortices become unstable and exotic shedding patterns may appear. The present numerical results demonstrate that the oblique shocks generated near the blade trailing edge oscillate at the same frequency of the vortices. In some cases the vortex shedding disappears. Trailing edge continuous cooling changes the vortex shedding pattern since the base region is separated into two different zones and two separated couples of vortices appear (Fig. 14). In both cases, the shedding of a single vortex on one side, and a pair of vortices on the other side of the trailing edge described by Williamson and Roshko [28] was identified. Frequency analysis of the base region demonstrated that both regions are tuned with each other but with a different energy

distribution within the spectrum. Hence, the vortices have the same harmonics but the amplitudes of their fluctuations are different.

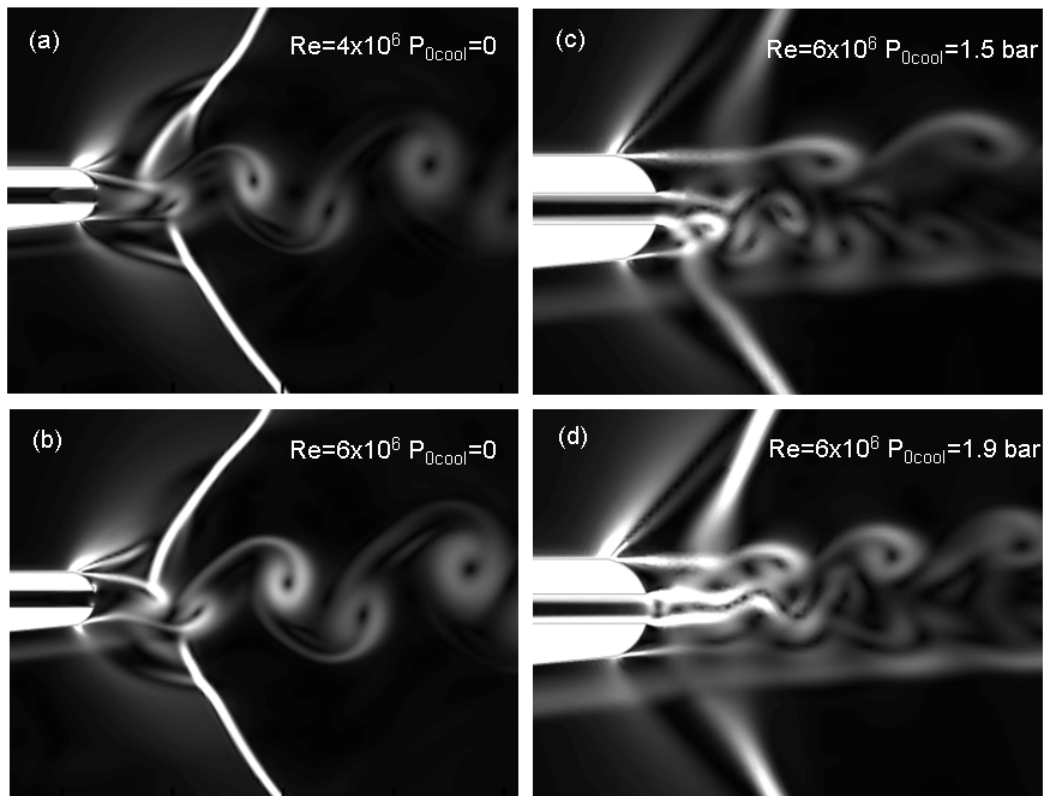


**Fig. 14.** Numerical Schlieren of the base region at  $M_{2,is}=1.1$

Fig. 15 represents the FFT of the trailing edge pressure sensors, which reveal the resonance frequencies associated to the shedding frequency. One observes that as the flow velocity increases, the shedding frequency is larger. A decrease in the shedding frequency is encountered with increasing Reynolds number owing to the reduction in total temperature and thus on velocity.

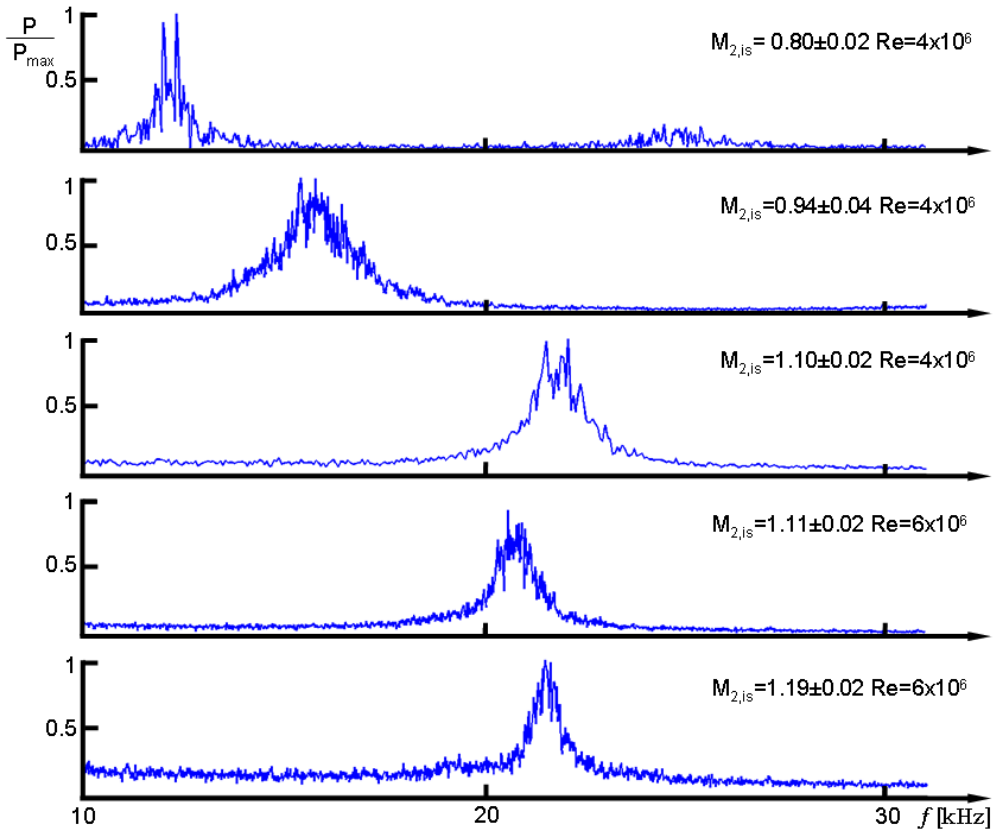


**Fig. 15.** Frequency spectrum of the unsteady base pressure signal for the uncooled case

The fluctuations in the base pressure, caused by the vortex shedding, are of the order of 5% in uncooled case and 13% for the pulsating cooling. Cicitelli and Sieverding [13] observed a 5% fluctuation in their uncooled geometry. URANS simulations in an uncooled transonic turbine stage [4] provided a 5% variability in the stator base pressure. Based on the experimental and numerical shedding frequencies let us define the Strouhal number:  $St=fL/v$ . Fig. 16 displays the evolution of the Strouhal number in function of the isentropic Mach number. The frequencies obtained from experimental and numerical analysis show good agreement with the tabulated data of Motallebi and Norbury [14]. The Strouhal numbers for the  $M_{2,is}=1.2$  case with continuous cooling of  $P_{0,cool} = 1.1$  bar and 1.5 bar are 0.23 and 0.18 respectively, based on the real dimension of the upper/lower metal part of the trailing edge. At a certain distance from the trailing edge the structures coalesce into a single couple of vortices. An increase in Strouhal number is observed for low coolant blowing cases throughout the whole Mach number range. This is due to the displacement of the vortex formation location downstream when the highest base pressure is observed [14]. Augmentation in coolant ejection rates brakes down the base region into two separate parts on each side of the trailing edge and, consequently, leads formation of two distinct vortex structures with higher frequencies as visualized in Fig. 14-c. CFD allowed the identification of high Strouhal numbers for the case of high cooling rates ( $St\sim 0.65$ ).

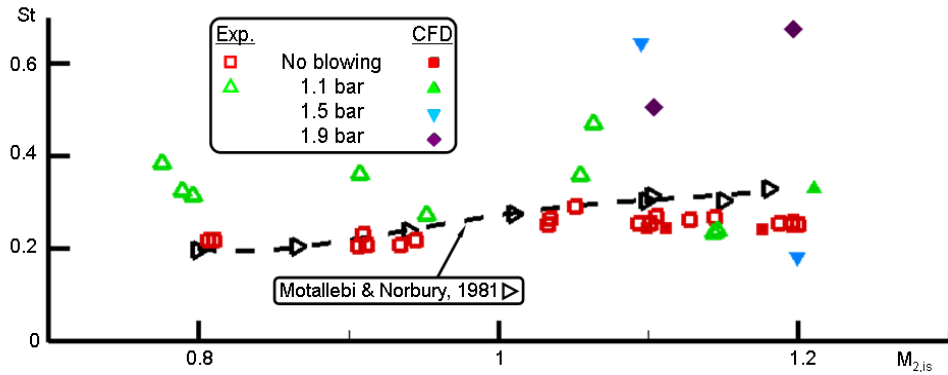


Fig. 16. Strouhal number evolution for various test conditions

### 5.2. Base pressure correlation

The base pressure values as a function of outlet Mach numbers are tabulated in Fig. 17. Lines represent the Sieverding's correlation [9]. In convergent designs,  $\delta$  represents the trailing edge wedge angle,  $\varepsilon$  is the suction side curvature downstream of the throat. The results of the uncooled measurements fit quite well with the correlation belonging to converging-diverging passages. Data obtained with coolant blowing at 1.1 bars fits the Sieverding's correlation equivalent to a  $(\varepsilon+\delta)/2=8$ . Coolant blowing results in an increase of base pressure. The highest increase in base pressure is achieved when the blowing ratio is the lowest. Hence, appropriate use of cooling is similar to morphing the airfoil. Slight changes in cooling rate results in base pressures of different airfoil geometries that one can predict using Fig. 17. Base pressure is observed to be maintained on the same level of the continuous cooling for the pulsating coolant ejection. This implies that the order of the accumulated losses is reduced by unsteady cooling.

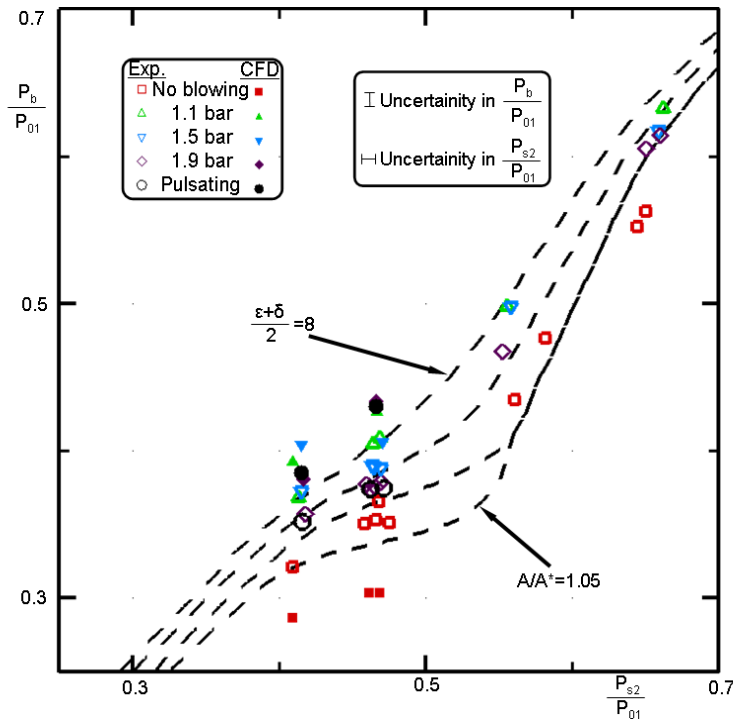


Fig. 17. Base pressure for all test cases together with Sieverding's correlation [9]

## 6. Conclusions

A transonic turbine airfoil was experimentally and numerically tested to resolve the effects of pulsating cooling. The model was tested at four Mach numbers (0.8, 0.95, 1.1, and 1.2), and two engine representative Reynolds numbers ( $4 \times 10^6$  and  $6 \times 10^6$ ).

The detrimental effects of the trailing edge shock waves on the neighboring airfoil and downstream plane are reduced with coolant ejection. The highest reduction is achieved with pulsating cooling. The Reynolds number stabilized the shock angle, minimized the RMS. Pulsating cooling ejection results in shock waves less oblique with significantly lower RMS values. A detailed investigation of the flow topology at the base region shows the modes of vortex shedding for different main flow and cooling conditions. The frequency of the vortex shedding is increased by introducing coolant which first pushes the vortex formation location downstream and at high ejection rates divides the base region into two.

Surface temperatures were extracted on the suction side by using fast response thin film gauges. Nusselt number distributions were extracted to designate the location of boundary layer transition. Unsteadiness associated with blade temperature were reported in terms of signal RMS. The result of the analyses shows significant agreement and complements each other in determination of the inclination and the intensity of the shock waves changing with cooling condition. It has been observed that the shock angle is increased and intensity is decreased by increasing coolant ejection pressure within the range of interest. The highest improvement in terms of the impact on the neighboring airfoil is attained with pulsating cooling. In addition, the stabilizing effect of pulsating coolant ejection is observed on boundary layer unsteadiness.

Base pressure is observed to be highly affected by the base bleed. The value is increased the most by a low coolant ejection rate. Pulsating cooling maintains the base pressure at the same level of the continuous cooling with the same average ejection pressure. The impact of cooling on wake unsteadiness for various Mach and Reynolds numbers are quantified in terms of the Strouhal number.

The present novel research on control of the shock waves presents the influence of unsteady trailing edge coolant ejection on the modulation of shock waves. The potential implementation of the proposed cooling scheme in turbine applications might lead to turbine efficiency and life-span increase. Furthermore, the present results should provide aerodynamic designers new tools to harness shock interactions.

## References

- [1] S. Djouimaa, L. Messaoudi, P.W. Giel, Transonic turbine blade loading calculations using different turbulence models – effects of reflecting and non-reflecting boundary conditions, *Appl. Therm. Eng.* 27 (2007) 779-787.
- [2] J.D. Denton, L. Xu, The Trailing Edge Loss of Transonic Turbine Blades, *ASME J. of Turbomach.* 112 (119) 277-285.
- [3] J.D. Denton, Loss Mechanisms in Turbomachinery, *ASME J. of Turbomach.* 115 (1993) 621-656.
- [4] G. Paniagua, T. Yasa, A. de la Loma, L. Castillon, T. Coton, Unsteady strong shock interactions in a transonic turbine: Experimental and numerical analysis, *J. of Propuls. and Power* 24 (2008) 722-731

- [5] J.P.Gostelow, A. Mahallati, S.A. Andrews, W.E. Carscallen, Measurement and Computation of Flowfield in Transonic Turbine Nozzle Blading With Blunt Trailing Edges, ASME Paper No. GT2009-59686, in: Proc. of ASME Turbo Expo 2009: Power for Land, Sea and Air, June 8-12, Orlando, FL, 2009
- [6] O. Uzol, C. Camci, B. Glezer, Aerodynamic Loss Characterization of a Turbine Blade with Trailing Edge Coolant Ejection: Part I – Effect of Cut-Back Length, Spanwise Rib Spacing, Free-Stream Reynolds Number and Chordwise Rib Length on Discharge Coefficients, ASME J. of Turbomach. 123 (2001) 238-248.
- [7] O. Uzol, C. Camci, Aerodynamic Loss Characterization of a Turbine Blade with Trailing Edge Coolant Ejection: Part II – External Aerodynamics, Total Pressure Losses and Predictions, ASME J. of Turbomach. 123 (2001) 249-257.
- [8] M.T. Schobeiri, K. Pappu, Optimization of Trailing Edge Ejection Mixing Losses: A Theoretical and Experimental Study, J. of Fluid Eng. 121 (1999) 118-125.
- [9] C.H. Sieverding, M. Stanislas, J. Snoeck, The Base Pressure Problem in Transonic Turbine Cascades, J. of Eng. for Power, 102 (1980) 711-718.
- [10] A. Rowe, A.L.A. Fry, F. Motallebi, Influence of Boundary Layer Thickness on Base Pressure and Vortex Shedding Frequency, AIAA J. 39 (2000) 754-756.
- [11] C.H. Sieverding, H. Heinemann, The influence of boundary layer state on vortex shedding from flat plates and turbine cascades, ASME J. of Turbomach. 112 (1990) 181-187.
- [12] K. Vassilopoulos, S.L. Gai, Unsteady Base Flow – Vortex Shedding and Pressure Fluctuations, AIAA-1996-1957, in: Proc. of the 20th Congress of the International Council of the Aeronautical Sciences, Sep. 8-13, Napoli, Italy, 1996.
- [13] G. Ciccotelli, C.H. Sieverding, The Effect of Vortex Shedding on the Unsteady Pressure Distribution Around the Trailing Edge of a Turbine Blade, ASME J. of Turbomach. 119 (1997) 810-819.
- [14] F. Motallebi, J.F. Norbury, The Effect of Base Bleed on Vortex Shedding and Base Pressure in Compressible Flow, J. of Fluid Mech. 110 (1981) 273-292.
- [15] C.H. Sieverding, The influence of Trailing Edge Ejection on the Base Pressure in Transonic Turbine Cascades, ASME J. of Eng. for Power 105 (1983) 215-222.
- [16] M. Raffel and F. Kost, Investigation of Aerodynamic Effects of Coolant Ejection at the Trailing Edge of a Turbine Blade Model by PIV and Pressure Measurements, Exp. in Fluids. 24 (1998) 447-461.
- [17] B.H. Saracoglu, G. Paniagua, P. Rambaud, Blunt Trailing Edge Cooling Effects at Supersonic Regime, AIAA-2009-5105, in: Proc. of 45th AIAA/ASME/SAE&ASEE Joint Propulsion Conference, Aug. 2-5, Denver, CO, 2009.
- [18] A. de la Loma, G. Paniagua, D. Verrastro, P. Adami, Transonic turbine stage heat transfer investigation in presence of strong shocks, ASME J. of Turbomach. 130 (2008) 031019.
- [19] J.P. Solano, V. Pinilla, G. Paniagua, S. Lavagnoli, T. Yasa, Aero-thermal investigation of a multi-splitter axial turbine, Int. J. of Heat and Fluid Flow, 32 (2011) 1036-1046.
- [20] C.H. Sieverding, T. Arts, R. Dénos, F. Martelli, Investigation of the Flow Field Downstream of a Turbine Trailing Edge Cooled Nozzle Guide Vane, ASME J. of Turbomach. 118 (1996) 291-300.

- [21] T.V. Jones, D.L. Shultz, A.D. Hendley, On the Flow in an Isentropic Free Piston Tunnel, ARC R&M 3731, 1973.
- [22] D.L. Shultz, T.V. Jones, M.L.G. Oldfield, L.C. Daniels, A new transient facility for the measurement of heat transfer rates in “High Temperature Problems in Gas Turbine Engines”, AGARD CP-229, 1978.
- [23] M. Gonzalez, G. Paniagua, B. Saracoglu, A. Tiseira, Pulsating cooling system for high-pressure turbine blades, AIAA-2010-4587, in: Proc. of the 5th AIAA Flow Control Conference, June 28-1, Chicago, IL, 2010.
- [24] G.S. Settles, Schlieren and Shadowgraph Techniques: Visualizing Phenomena in Transparent Media, Springer-Verlag, Berlin, 2001.
- [25] F.R. Menter, Zonal Two Equation  $k-\omega$  Turbulence Models For Aerodynamic Flows. AIAA-1993-2906. in: Proc. of 23rd Fluid Dynamics, Plasmadynamics, and Lasers Conference, July 6-9, Orlando, FL, 1993.
- [26] B. Saracoglu, P.G. Huang, and G. Paniagua, Numerical Study of a Transonic Linear Cascade for Pulsating Trailing Edge Cooling Research, in Proc: 10th Int. Symposium on Experimental Computational Aerothermodynamics of Internal Flows, Brussels, 2011.
- [27] J.P. Gostelow, M.F. Platzer, W.E. Carscallen, On Vortex Formation in the Wake Flows of Transonic Turbine Blades and Oscillating Airfoils, ASME J. of Turbomach. 128 (2006) 528-535.
- [28] C.H.K. Williamson, A. Roshko, Vortex Formation in the Wake of an Oscillating Cylinder, J. Fluids and Struct. 2 (1988) 355–381.